Journal of Theoretical and Applied Physics (JTAP), Vol.16, No. 2, 162216 (1-6), 2022
Received 25 March 2022 ; Accepted 30 April 2022 ; [http://dx.doi.org/10.30495/jtap.162216]

Effect of transverse wiggler magnetic field on the growth rate of Raman backscattering of X-mode laser in rippled density plasma

Manish Dwivedi , Hitendra K. Malik*

Abstract
A problem of Raman backscattering of laser beam propagating in a transversely wiggler magnetized plasma is considered in the presence of density ripples. Required dispersion relation of excited upper hybrid wave is derived by using the fluid model and taking into account the coupling between primary upper hybrid wave and density ripples. Using wave equation and nonlinear ponderomotive force and considering the coupling between the sideband wave and the upper hybrid wave, an expression of growth rate of this instability is obtained. The calculations demonstrate that the growth rate decreases by increasing the external magnetic field since the coupling between the scattered wave and upper-hybrid wave is weak and phase matching condition is not well-satisfied for higher external magnetic field. We have observed that instability is suppressed due to the presence of density ripples. Also, the suppression is significant for the case of small wave number density ripples as large faction of energy of upper hybrid electron wave transfers to the secondary hybrid electron wave.

Keywords
Raman scattering (RBS), Wiggler field, UHW, Growth rate, Suppression of instability.

Plasma Science and Technology Laboratory, Department of Physics, Indian Institute of Technology Delhi, New Delhi-110016, India.
***Corresponding author**: hkmalik@physics.iitd.ac.in

1. Introduction

Stimulated Raman scattering (SRS) is a parametric instability in which a pump laser (ω_0, k_0) decays resonantly into an electron plasma (ω, k) wave and a scattered electromagnetic wave (ω_s, k_s) with a shifted frequency. The necessary condition for the feasibility of the phenomenon can be expressed by the wavenumber and frequency matching condition:

$$\mathbf{k}_0 = \mathbf{k} + \mathbf{k}_s, \omega_0 = \omega + \omega_s$$

The scattered electromagnetic wave and pump laser produce nonlinear ponderomotive force at their beating frequency and wavenumber, which amplifies the electron plasma wave. The amplified plasma wave and pump laser produces nonlinear current density at (ω_s, k_s). This feedback mechanism leads to the exponential growth of scattered EM until the waves don't get saturate in the plasma due to other nonlinear phenomena. The large amplitude plasma wave generated in this process leads to the partial disintegration of the laser pump energy into the plasma. Raman scattering and other mode conversion phenomena such as Brillouin scattering [1] arise in the laser-plasma interaction resulting in inefficient laser-plasma coupling. This makes the practical implementation of laser-plasma interaction such as inertial confinement [2], harmonic generation [3], THz generation [4], and plasma-based accelerators [5] more challenging. In Inertial confinement fusion (ICF), the outer region of the pellet turns into plasma, scattering of the pump laser prevents energy from reaching the critical density for the resonance absorption [6]. Hence, it is essential to study the phenomena which can lead to the inhibition of scattering of the wave. There are several advancements for minimizing the growth rate of such parametric instabilities, such as laser smoothing techniques [7], increasing laser bandwidths [8], high initial plasma temperature [9].
The presence of stationary density ripples $n_e^q = n_0 \eta \cos qz$ introduces spatial inhomogeneity in plasma, here n_0 is equilibrium density, η and q are relative amplitude and wavenumber of density ripples. There are methods such as Langmuir wave decay (LDI) [10], two-plasmon decay [11], through which density ripples can be generated in plasma. Another method of generating density ripples is the incident of sound waves on a neutral gas which is further ionized by the laser beam [12]. The interaction of upper hybrid electrons waves couples with the stationary electron density ripples and produce the other electrostatic modes $(\omega, k + mq)$ of the same frequency and higher wavenumber, m is an integer. It has been exhibited that this process has no threshold parameters [13]. However, in the weak-coupling limit $\eta \omega_p^2 \approx 3q^2 v_{th}^2$, it is reasonable to consider the three-wave interaction, i.e., $m = \pm 1$; here $v_{th} = (3KT/m_e)^{1/2}$ is the thermal speed of electrons and K and T are Boltzmann constant and electron temperature, respectively together with m_e is electron mass [13]. Wang and Feng et al. studied the effects of static sinusoidal density modulation on the growth rate of backward stimulated Ra-

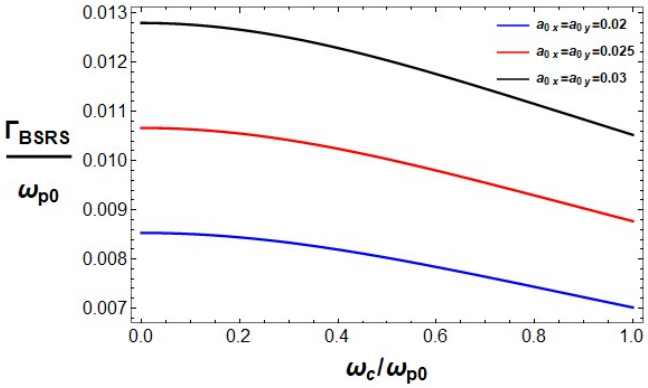

Figure 1. variation of growth rate with the normalized cyclotron frequency for different value of normalized laser strength a_0.

man scattering (BSRS) by kinetic theory and Vlasov stimulation [14]. They observed the transition of SRS from absolute to a convective instability through density modulation. It has been shown that the ions oscillation can reduce the effects of density modulation; consequently, the growth rate of BSRS is high as compared to a fixed ions case. Pathak and Tripathi have found suppressing SRS of laser propagating in rippled density plasma up to 50% at rippled amplitude 40% [15]. They considered the density ripples formed by the counter-propagating laser beams. Zhao et al. have examined the hindrance of SRS due to the excitation of stimulated Brillouin scattering (SBS) [16]. They derived a threshold of plasma density perturbation due to SBS for SRS inhibition. It has been shown through the PIC simulations that this condition can be achieved easily by SBS in the fluid regime, with $k\lambda_D < 0.15$. But the study of Pathak and Wang constrained to the situation when the wavenumber of ripple density is $\approx 2k_0$.

In the present paper, we have investigated the Raman backscattering of laser in transverse wiggler magnetized plasma using the fluid model and considering the coupling of upper hybrid electron wave and pre-existing density ripples of arbitrary wavenumber of arbitrary wavenumber. The main objective of the current work is to study the combined effects of stationary density ripples and transverse wiggler magnetic fields. Our investigation is confined to the backward stimulated Raman scattering as its growth rate is prominent in fluid regime i.e., $k\lambda_D < 0.3$ which makes the study relevant to experimental investigation.

2. Coupling of primary and secondary upper hybrid waves

We have considered plasma irradiated by a laser beam with the following electric field profile

$$\mathbf{E}_0 = (E_{0x}\hat{x} + \alpha E_{0y}\hat{y} + E_{0z}\hat{z})e^{-i(\omega_0 t - k_0 z)} \quad (1)$$

We have considered the plasma with equilibrium density n_0 and a pre-existing density ripple $n_0\eta\exp(iqz)$, here η and q is relative amplitude and wavenumber of density ripples, respectively. In addition, the plasma is immersed in the wiggler magnetic field having a profile

$$\mathbf{B}_0 = B_h(\cos k_b z\hat{x} + \sin k_b z\hat{y})$$

The incident electromagnetic wave undergoes the phenomena of stimulated Raman scattering causes the generation of a backward scattered electromagnetic wave

$$\mathbf{E}_s = (E_{sx}\hat{x} + \alpha E_{sy}\hat{y} + E_{sz}\hat{z})e^{-i(\omega_s t + k_s z)} \quad (2)$$

and an electrostatic plasma wave

$$\Phi_{\omega,k} = \phi_{\omega,k}e^{-i(\omega t - kz)} \quad (3)$$

Here, the conservation of momentum and energy requires the following conditions

$$k_0 = k_s + k$$

$$\omega_0 = \omega_s + \omega$$

The oscillator velocity impart from the high-frequency electromagnetic wave is

$$\mathbf{v}_j = \frac{-ie\omega_j^2}{2m_e\omega_j(\omega_j^2 - \omega_h^2)}$$

$$(2E_{jx}(1 - \frac{\omega_h^2}{\omega_j^2}\cos^2 k_b z) - E_{jy}\frac{\omega_h^2}{\omega_j^2}\sin 2k_b z + 2iE_{jz}\frac{\omega_h}{\omega_j}\sin k_b z)\hat{x}$$

$$+(-E_{jx}\frac{\omega_h^2}{\omega_j^2}\sin 2k_b z + 2E_{jy}(1 - \frac{\omega_h^2}{\omega_j^2}\sin^2 k_b z - iE_{jz}\frac{\omega_h}{\omega_j}\cos k_b z))\hat{y}$$

$$+(-2iE_{jx}\frac{\omega_h}{\omega_j}\sin k_b z + 2iE_{jy}\frac{\omega_h}{\omega_j}\cos k_b z + 2E_{jz})$$

Here j=0 and s. The incident and scattered laser also exerted ponderomotive force at their beating frequency and wavenumber (ω, k) given by

$$\mathbf{F}_p = e\nabla\Phi_{p\omega k}$$

Here ponderomotive potential is

$$\Phi_{p\omega k} = \frac{-e}{2m_e\omega_0\omega_s}\mathbf{E}_0 \cdot \mathbf{E}_s^*$$

The response of electrons to the ponderomotive potential $\Phi_{p\omega k}$ and self-consistent potential $\Phi_{\omega k}$ is governed by the equation of motion, from which we obtained the (ω, k) component of electron velocity

$$\mathbf{v}_{\omega,k} = \frac{-iek(\Phi_{p\omega k} + \Phi_{\omega k})\omega_h}{m(\omega^2 - \omega_c^2)}(\sin k_b z\hat{x} - \cos k_b z\hat{y} - \frac{\omega}{\omega_h}\hat{z}) \quad (4)$$

The electron velocity component (ω,k) couples with the stationary electron rippled density leads to the density perturbation at $(\omega,k_2=k+q)$. The density perturbation at (ω,k_2) is governed by Poisson's equation $\varepsilon_0\nabla^2=en_{\omega,k_2}$ and the continuity equation

$$\frac{\partial n_{\omega,k_2}}{\partial t}+\nabla\cdot(n_0\mathbf{v}_{\omega,k_2}+\frac{1}{2}n_e^q\mathbf{v}_{\omega,k})=0 \tag{5}$$

Here $\mathbf{v}_{(\omega,k_2)}$ can be obtained from the equation of motion

$$m_en_0\frac{\partial\mathbf{v}_{\omega,k_2}}{\partial t}=-en_0\nabla\Phi_{\omega,k_2}-e(\mathbf{v}_{\omega,k2}\times\mathbf{B}_0)-\frac{5}{2}KT_e\nabla n_{\omega,k_2}$$

Which gives

$$\mathbf{v}_{\omega,k_2}=\frac{-iek(1+\delta)\omega_c}{m\omega(\omega^2-\omega_h^2)}$$

$$(\Phi_{\omega k_2}-\frac{5ev_{th}^2n_{\omega,k_2}}{6\varepsilon_0\omega_{p0}^2})(-\sin k_bz\hat{x}+\cos k_bz\hat{y}+\frac{i\omega}{\omega_h}\hat{z}) \tag{6}$$

On solving Eqs. 5 and 6 simultaneously, one can obtain the expression of n_{ω,k_2}. After substituting n_{ω,k_2} in the Poisson's equation, we obtained the following equation

$$\Phi_{\omega k_2}=-\beta(\Phi_{p\omega k}+\Phi_{\omega k}) \tag{7}$$

$$\beta=\frac{\omega_{pq}^2}{2(1+\delta)(\omega^2-\omega_h^2-\omega_{p0}^2-\frac{5}{6}k^2v_{th}^2(1+\delta)^2)} \tag{8}$$

Here $\omega_{pq}^2=\eta\omega_{p0}^2$ and $\delta=q/k$. Equation 8, represents the coupling of secondary hybrid plasma wave (LHS) and primary hybrid plasma wave (RHS). It is noticeable that coupling of upper hybrid plasma wave with secondary hybrid plasma wave is because of the electron density ripples. The constant term β on RHS represents the coupling factor of the primary and secondary waves. The velocity component $\mathbf{v}_{\omega,k_2}$ couples with stationary rippled density and produces nonlinear current $\mathbf{v}_{\omega,k_2}n_e^{q*}/2$, which perturbed the electron density at ω,k. The density perturbation $n_{\omega,k}$ is governed by Poisson's equation $\varepsilon_0\nabla^2\Phi_{\omega,k}=en_{\omega,k}$ and continuity equation

$$\frac{\partial n_{\omega,k}}{\partial t}+\nabla\cdot(n_0\mathbf{v}_{\omega,k}+\frac{1}{2}\mathbf{v}_{\omega,k_2}n_e^{q*})=0$$

Using these equations, we obtain

$$\varepsilon_{\omega,k}\Phi_{\omega,k}=-\chi_{\omega,k}\Phi_{p\omega,k} \tag{9}$$

Here,

$$\varepsilon_{\omega,k}=1-\frac{\omega_{p0}^2}{\omega^2-\omega_h^2}-\frac{\beta\omega_{pq}^2(1+\delta)(\omega_{p0}^2+\frac{5}{6}k^2v_{th}^2(1+\delta)^2)}{2\omega(\omega^2-\omega_h^2)\omega_{p0}^2}$$

And $\chi_{\omega,k}=\varepsilon_{\omega,k}-1$. The equation for the electrostatic wave is determined by using Poisson's equation Eq. 9 can be rewritten in the following way

$$\varepsilon_{\omega,k}\Phi_{\omega,k}=\frac{e\chi_{\omega,k}}{2m_e\omega_s\omega_0}\mathbf{E}_0\cdot\mathbf{E}_s^* \tag{10}$$

3. Derivation of growth rate

The wave equation of the scattered EM wave is

$$\nabla^2\mathbf{E}_s-\nabla(\nabla\cdot\mathbf{E}_s)+\frac{\omega_s^2}{c^2}\mathbf{E}_s=\frac{-i\omega_s\mathbf{J}_s}{c^2\in_0} \tag{11}$$

here $\mathbf{J}_s$ is the current density that drives the scattered wave. We expand the current density $\mathbf{J}_s$ as

$$\mathbf{J}_s=\mathbf{J}_s^L+\mathbf{J}_s^{NL} \tag{12}$$

Together with $\mathbf{J}_s^L$ as the linear current density due to $\mathbf{v}_s$ and $\mathbf{J}_s^{NL}$ as the nonlinear current density arose due to the coupling between $\mathbf{v}_s$ and density perturbation $n_{\omega k}^*$. These are

$$\mathbf{J}_s^L=-en_0\mathbf{v}_s\&\mathbf{J}_s^{NL}=\frac{-en_{\omega k}^*\mathbf{v}_0}{2} \tag{13}$$

The Fourier analysis of the wave equation of scattered electromagnetic wave give rise to the following relation

$$\mathbf{D}\cdot\mathbf{E}_s=\frac{ek^2\Phi_{\omega k}^*}{2m_e\omega_0\omega_s(\omega_0^2-\omega_h^2)}\mu\cdot\mathbf{E}_0 \tag{14}$$

Where D is the dispersion tenor

$$D=\begin{bmatrix}A & B & -iF\sin k_bz\\ B & D & iF\cos k_bz\\ iF\sin k_bz & -iF\cos k_bz & G\end{bmatrix}$$

$$A=\frac{\omega_s^2(\omega_s^2-\omega_{p0}^2-\omega_h^2)+\omega_h^2\omega_{p0}^2\cos^2k_bz}{\omega_s^2(\omega_s^2-\omega_h^2)}-k^2$$

$$B=\frac{\omega_h^2\omega_{p0}^2\sin k_bz\cos k_bz}{\omega_s^2(\omega_s^2-\omega_h^2)}$$

$$F=\frac{\omega_h\omega_{p0}^2}{\omega_s(\omega_s^2-\omega_h^2)}$$

$$D=\frac{\omega_s^2(\omega_s^2-\omega_{p0}^2-\omega_h^2)+\omega_h^2\omega_{p0}^2\sin^2k_bz}{\omega_s^2(\omega_s^2-\omega_h^2)}-k^2$$

$$G=\frac{\omega_s^2-\omega_{p0}^2-\omega_h^2}{(\omega_s^2-\omega_h^2)}$$

Here $k=k_sc/\omega_s$ and,

$$\mu=\begin{bmatrix}a_0 & b_0 & c_0\\ a_1 & b_1 & c_1\\ a_2 & b_2 & c_2\end{bmatrix}$$

$a_0=-\omega_0^2+\omega_h^2\cos^2k_bz$, $b_0=\omega_h^2\sin k_bz\cos k_bz$, $c_0=-i\omega_0\omega_h\sin k_bz$

$$a_1 = \omega_h^2 \sin k_b z \cos k_b z\ ,\ b_1 = -\omega_0^2 + \omega_h^2 \sin^2 k_b z\ ,\ c_1 = i\omega_0\omega_h \cos k$$

$$a_2 = i\omega_0\omega_h \sin k_b z\ ,\ b_2 = -i\omega_0\omega_h \cos k_b z\ ,\ c_2 = -\omega_0^2$$

From Eq. 14, we have

$$\mathbf{E}_s = \frac{ek^2\Phi^*_{\omega k}}{2m_e\omega_0\omega_s(\omega_0^2-\omega_c^2)}\mathbf{D}^{-1}\cdot(\mu\cdot\mathbf{E}_0)$$

$$\mathbf{E}_s = \frac{ek^2\Phi_{\omega k}}{2m_e\omega_0\omega_s(\omega_0^2-\omega_c^2)}\frac{Adjoint(D)}{|D|}\cdot(\mu\cdot\mathbf{E}_0) \quad (15)$$

Here $|D|$ is the determinant of matrix $\mathbf{D}$. Using Eq. 10 and 15, we obtain

$$\varepsilon^*_{\omega,k}|\mathbf{D}| = \frac{-e^2k^2\chi^*_{\omega,k}}{4m_e^2\omega_0^2\omega_s^2(\omega_s^2-\omega_h^2)}\mathbf{E}^*_0\cdot(Adjoint(\mathbf{D})\cdot(\mu\cdot\mathbf{E}_0)) \quad (16)$$

The dispersion relation (16) exhibits how the electrostatic wave and scattered EM wave are coupled through the pump laser and plasma. Equation 16, in the absence of the pump, yields $|\mathbf{D}| = 0$ and $\varepsilon_{\omega k} = 0$, giving linear eigen modes of the plasma. In a resonant three wave parametric process we look for a solution to dispersion relation near the simultaneous zero of $|\mathbf{D}|$ and $\varepsilon_{\omega k}$. Thus, we expanded $\varepsilon_{\omega k}$ and $|\mathbf{D}|$ about the eigen-frequencies ω_r and $\omega_{rs}$to get the growth rate

$$\Gamma^2_{SRS} = \frac{-e^2k^2\chi^*_{\omega,k}}{4m_e\omega_0^2\omega_s^2(\omega_s^2-\omega_c^2)\frac{\partial\varepsilon_{\omega k}}{\partial\omega}|_{\omega_r}\frac{\partial|D|}{\partial\omega_s}|_{\omega_{rs}}}$$

$$\mathbf{E}^*\cdot(Adjoint(\mathbf{D}\cdot(\mu\cdot\mathbf{E}_0))) \quad (17)$$

4. Results and discussion

We have have numeriaclly calculated and plotted the average growth rate over the proportion distance $\bar{\Gamma}_{SRS} = \int_0^L \Gamma_{RSR}dz/\int_0^L dz$ where L is the length of plasma. The numerical and simulation approaches have proved to be very effective in different areas [17–19].

In figure. 2, we plotted the variation of the normalized electrostatic potential of secondary upper hybrid wave with normalized wave number of density ripples for different relative density ripples amplitude values. One can observe the amplitude of electrostatic potential of secondary upper hybrid wave decreases with the relative wave number of density ripples and increases with the relative amplitude of density ripples. This is because coupling between the primary and secondary wave becomes relatively weakened as the wave number of density ripples increases. Also, coupling get stronger with the relative amplitude of density ripples.

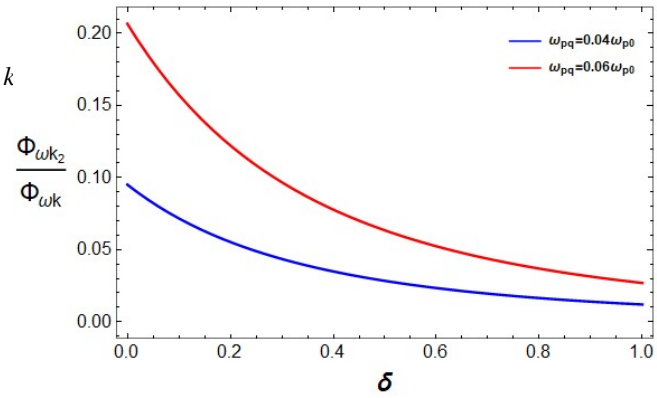

Figure 2. Variation of $\Phi_{\omega k_2}/\Phi_{\omega k}$ with relative wave number δ of density ripples for different values of relative density ripples amplitude ω_{pq}0.04 and 0.06.

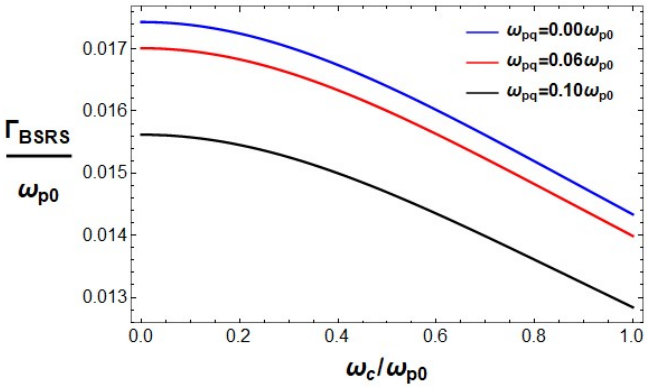

Figure 3. Variation of the normalized growth rate of Raman backscattering with the normalized cyclotron frequency for different values of the relative amplitude of density ripples ($a_{0x} = a_{0y} = 0.02$).

In figure. 1, we plotted the variation of growth rate with the normalized cyclotron frequency for different normalized laser amplitude $a_{0j} = eE_{0j}/m\omega_0 c$ and $\omega_0 = 0.2\omega_{p0}$ in uniform density plasma together with wiggler wave number k_b=50 and plasma length L=10 cm. The plasma temperature is taken T_e=2.5keV and kc/ω_{p0}=0.8. The growth rate decreases with the increasing magnetic field. The reason is that the upper hybrid frequency increases by increasing the cyclotron frequency and this results in the reduction in frequency of the scattered sideband wave, therefore the phase matching condition for the Raman backscattering instability cannot be appreciably fulfilled, and hence, the growth rate decreases with the increasing magnetic field. Also, the growth rate is sensitive to the normalized laser amplitude.

Figure 3 shows the variation of the normalized growth rate of Raman backscattering with the normalized cyclotron frequency for different relative amplitude of density ripples values. Here, we have taken laser strength $a_{0x} = a_{0y} = 0.02$ and the rest of the parameters are same. The variation of growth rate with the normalized cyclotron frequency in density rippled plasma is similar to that of in uniform density plasma.

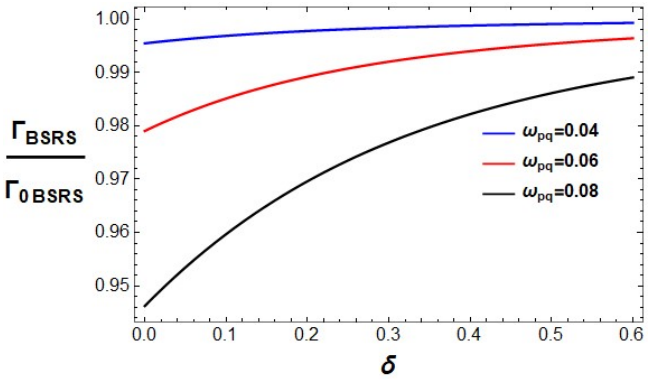

Figure 4. Variation of the relative growth rate with the relative wave number of density ripples for different values of the relative amplitude of density ripples.

However, there is a scalar down shift in the growth rate of Raman backscattering in the cases of density ripple plasma which exhibits the inhibition of instability due to density ripples. It is found that hindrance to instability enhances with the relative amplitude of density ripple ω_{pq}. We have observed around 10.41% suppression of growth rate of Raman backscattering due to the presence of density ripples of relative amplitude and wavenumber $0.01\omega_{p0}$ and 0.2, respectively. It is also noticeable that the variation of scalar difference between the growth rates of instability for two different density ripples amplitude is independent of the external magnetic field. This is because, in our theoretical analysis we found that coupling between primary wave and secondary wave have negligible dependence on the external magnetic. Hence, the presence of density ripples only decreases the growth rate of instability, it does not affect the dependence of growth rate on the external magnetic field.

Figure 4 discusses the variation of the relative growth rate with the relative wave number of density ripples for different values of the relative amplitude of density ripples. It is noticeable that relative growth rate increases with the relative wave number of the density ripples. Hence, the suppression of Raman backscattering is insignificant in the cases of larger wavenumber density ripples. This is because large δ lead to the transfer of a small fraction of energy of the primary wave to the secondary wave. Also, Raman backscattering is significantly suppressed in the larger amplitude density ripple plasma.

We have seen the impact of relative wave number of density ripples, amplitude of density ripples and cyclotron frequency on the growth rate of the Raman backscattering of X-mode laser for different strength of the laser intensity and fixed profile of the beam in a plasma. However, with other profiles that have proved to be useful in optics [20, 21] this mechanism could find more interesting results [22]. This would be our next objective to work upon.

5. Conclusion

The calculations showed that the coupling between upper hybrid wave and density ripples leads to the evolution of secondary upper hybrid wave, which carries a fraction of energy from the primary upper hybrid wave. This weakened the feedback mechanics of the parametric instability. Even small-amplitude rippled density can efficiently couple these waves. This is because small δ led to the transfer of a large fraction of energy of the primary wave to the secondary wave. Also, in the fluid regime the wavelength of the wiggler magnetic field does not have significant impact on the phenomena. In the limit $k\lambda_D > 0.3$, the growth rate of instability was found to be very small as the Landau damping is substantial in this limit [23]. Hence, one can expect insignificant impact of the density ripples on Raman backscattering. On the other hand, the suppression of instability due to density ripples was found to be independent of the wiggler magnetic field.

Conflict of interest statement:

The authors declare that they have no conflict of interest.

References

[1] C. Riconda and S. Weber. *High Power Laser Science and Engineering*, **4**, 2016.

[2] K. Burdonov, A. Soloviev, M. Starodubtsev, J. Fuchs, G. Revet, S.N. Chen, A. Eremeev, R. Osmanov, V. Ginzburg, E. Khazanov, A. Korzhimanov, A. Kuzmin, S. Pikuz, I. Shaykin, A. Shaykin, A. Sladkov, and I. Yakovlev. *International Conference Laser Optics*, :608, 2018.

[3] H. K. Malik and L. Devi. *Results in Physics*, **17**:103070, 2020.

[4] H. K. Malik. *Physics Letters A*, **384**:126304, 2020.

[5] S. Li, N. A. M. Hafz, M. Mirzaie, X. Ge, T. Sokollik, M. Chen, Z. Sheng, and J. Zhangb). *Journal of Applied Physics*, **116**:043109, 2014.

[6] P. Loiseau, O. Morice, D. Teychenné, M. Casanova, S. Hüller, and D. Pesme. *Physical review letters*, **97**:205001, 2006.

[7] Y. Zhao, S. Weng, Z. Sheng, and J. Zhu. *Plasma Physics and Controlled Fusion*, **61**:115008, 2019.

[8] Y. Zhao, J. Zheng, M. Chen, L. L. Yu, S. M. Weng, C. Ren, C. S. Liu, and Z. M. Sheng. *Physics of Plasmas*, **21**:112114, 2014.

[9] T Umeda and T Ito. *Physics of Plasmas*, **15**:84503, 2008.

[10] C. Z. Xiao, Z. J. Liu, C. Y. Zheng, and X. T. He. *Physics of Plasmas*, **23**:22704, 2016.

[11] J. Zhang, Z. Dai, and Z. Ren. *Journal of Physics D: Applied Physics*, **11**:231, 2000.

[12] N. A. Yampolsky and G. M. Fraiman. *Physics of plasmas*, **13**:113108, 2006.

[13] P. K. Kaw, A. T. Lin, and J. M. Dawson. *The Physics of Fluids*, **16**:1967, 1973.

[14] Y. X. Wang, Q. S. Feng, H. C. Zhang, Q. Wang, C. Y. Zheng, Z. J. Liu, and X. T. He. *Physics of Plasmas*, **24**:531, 2017.

[15] V. B. Pathak and V. K. Tripathi. *Physics of Plasmas*, **15**:22301, 2008.

[16] Y. Zhao, L. L. Yu, S. M. Weng, C. Ren, C. S. Liu, and Z. M. Sheng. *Physics of Plasmas*, **24**:92116, 2017.

[17] L. Malik and A. Tevatia. *Defence Science Journal*, **71**:137, 2021.

[18] L. Malik, S. Rawat, M. Kumar, and A. Tevatia. *Materials Today: Proceedings*, **38**:191, 2021.

[19] L. Malik, A. Escarguel, M. Kumar, A. Tevatia, and R. S. Sirohi. *Laser Physics Letters*, **18**:086003, 2021.

[20] L. Malik and A. Escarguel. *EPL (Europhysics Letters)*, **124**:64002, 2019.

[21] L. Malik. *Optics. Laser Technology*, **132**:106485, 2020.

[22] H. K. Malik. *Laser-Matter Interaction for Radiation and Energy*. CRC Press, 1th edition, 2021.

[23] M. Dwivedi and H. K. Malik. *IEEE Transactions on Plasma Science*, **50**:2, 2021.